Int. J. Nanosci. Nanotechnol., Vol. 15, No. 1, March. 2019, pp. 65-73

Short Communication

Synthesis and Characterization of Iron Oxide Nanoparticles by Thermal Decomposition Method of Iron (III) Chelates

Vidya Velayudhan Nair Girija* and Sadasivan Vasu

Department of Chemistry, Faculty of University College, Kerala University, M G Road, Palayam, Trivandrum-695034, Kerala, India.

(*) Corresponding author: vg_vidya@yahoo.co.in
(Received: 17 October 2017 and Accepted: 15 April 2018)

Abstract

Magnetic iron oxide nanoparticles have numerous applications in the biomedical field. This paper reports the preparation and properties of iron oxide nanoparticles synthesised by thermal decomposition method from iron chelates. The iron oxide nanoparticles were characterized by FTIR, powder XRD, VSM, SEM and TEM techniques. FTIR and powder XRD studies show that iron oxide was formed as α - Fe_2O_3 in its pure form. VSM study shows that the particles have got ferromagnetic property. XRD, SEM and TEM images show that the particles formed are in nanometre crystallite size.

Keywords: *Thermal decomposition, Nanoparticles, Iron chelates, Hematite, VSM, TG-DTG.*

1. INRODUCTION

Nanoscience and nanotechnology have gained significant momentum in recent years to interplay with biology and medical science, leads to the emergence of a new interdisciplinary field called nanomedicine [1]. Among different types of nano materials, magnetic iron oxide nanoparticles as magnetic resonance imaging contrast agents have set the most successful example for medical applications of inorganic nanoparticles. Various aspects of magnetic engineering to iron oxide nanoparticles ranging from chemical synthesis, magnetism engineering to *in vivo* applications have been published in recent years [2-9]. Magnetic iron oxide nanoparticles have many unique properties such as superparamagnetic, high coercivity, low Curie temperature, high magnetic susceptibility etc. Magnetic nanoparticles are of great interest for researchers from a broad range of disciplines including magnetic fluids, data storage, catalysis and bioapplications [10-14]. Currently magnetic nanoparticles are also used in important bioapplications including magnetic bioseperation and detection of biological entities, clinic diagnosis and therapy, targeted drug delivery and biological labels. The application of iron oxide nanoparticles in *in vitro* diagonostics has been practised for nearly half a century [2]. In the last decades increased investigations with several types of iron oxide have been carried out in the field of magnetic nanoparticles mostly include the α - Fe_2O_3, ϒ- Fe_2O_3, FeO, ε –Fe_2O_3, β- Fe_2O_3 and Fe_2O_3, among which maghemite is very promising in its biocompatibility. α - Fe_2O_3 is most widely used material in pigment, magnetic, biomedical and gas sensing applications [15]. In recent years many works are being done to synthesize nano sized Fe_2O_3 [16]. Non toxicity, low cost

and relatively good stability are attractive features of nano sized Fe_2O_3.

In last decades, much research have been carried out to synthesise iron oxide nanoparticles and many reports have come out describing efficient synthetic approaches to synthesise shape controlled, stable, biocompatible and monodispersed iron oxide nanoparticles [17,18]. Among the most common methods, thermal decomposition offers great advantages over the hydrolytic synthetic route regarding monodispersity as well as magnetic susceptibility of resultant particles [11-21]. Nano sized α - Fe_2O_3 shows unusual magnetic behaviour depending on the size and shape of α - Fe_2O_3 particles. Nano sized α-Fe_2O_3 having different shapes shows difference in their magnetic behaviour. Thus the effect of size and shape of α - Fe_2O_3 has got much attraction. Nano size distribution makes iron oxide particles nontoxic and biocompatible [22].

In this present work an attempt has been made to synthesise nanosized iron oxide particles from three different iron chelates by thermal decomposition method. The TG/DTG analysis of three newly prepared Fe(III) chelates were taken. The decomposition temperature of the iron chelates were found out from thermogram and iron oxides were prepared for each complex at their decomposition temperature by thermal decomposition method. The iron oxide obtained is characterized by various analytical techniques like FTIR, powder XRD and VSM measurements. The surface morphology of the obtained iron oxide were analysed using SEM and TEM techniques.

2. EXPERIMENTAL

All reagents and solvents for synthesis and analysis were Merck products and used as supplied. Thermogravimetric measurements of iron complexes were recorded in nitrogen atmosphere at heating rate of 10^{o}C/min on a TGA-50 analyzer. TG curves were recorded from ambient temperature to 1000^{o}C in an atmosphere at a linear heating rate of 10^{o}C/minute. FTIR spectra recorded using KBr discs on a Perkin-Elmer spectrum 65 spectrophotometer. FEG-SEM analysis of iron oxide residues obtained by heating the iron complexes just above their decomposition temperature were done on FEG-SEM JSM-7600F. TEM analysis of iron oxide residues were done on Philips CM 200/20-200 kV. VSM analysis of iron oxide residue were done on Lakeshore VSM 7410. The powder X-ray diffraction studies of iron oxide residues were done on Philips X-ray diffractometer (PW1710) using Cu K α (λ=1.5405Å) radiation.

The ligands were synthesized by usual diazotization procedure [23]. The three azo dye ligands prepared were 5-(2,3-dimethyl-1-phenyl-3-pyrazolin-5-one-4-ylazo)-1H-pyrimidine-2,4-dione (L^1) [24,25,26], 2-(2-hydroxynaphthalen-1-ylazo)-pyridin-3-ol (L^2) [27], 4-(2,4-dihydroxyphenylazo)-3-hydroxynaphthalene-1-sulfonic acid (L^3) [28, 29,30]. The complexes of L^1, L^2 and L^3 prepared by mixing ethanolic solutions of $FeCl_3$. $2H_2O$ and azo dyes in molar ratio 1:2. The solution obtained was heated under reflux for 6 hours for completion of reaction. The solid compound deposited was separated by suction filtration washed several times with ethanol and dried over silica gel in a desiccator. The complexes obtained were characterized by various spectral and analytical techniques.

The TG/DTG analysis of complexes were carried out on a simultaneous TG/DTG analyser in order to obtain a prior knowledge about the decomposition temperature of three different iron chelates. The decomposition temperature is different for different complexes and is obtained from their respective thermogram. In order to prepare iron oxide from their respective complex, a known mass of complex was taken in a silica crucible and subjected to pyrolysis at its decomposition temperature. The complexes were subjected to a

controlled heat treatment in a programmed muffle furnace. After firing the sample for 30 minutes, the residue was allowed to cool within the furnace and transferred to a desiccator. After attaining room temperature, the residue was weighed once again to confirm its stoichiometry. The sample was used for FTIR, powder XRD and VSM analysis for characterization. The surface morphology studied by SEM and TEM imaging.

3 RESULTS AND DISCUSSION

3.1 Thermal Analysis

Thermogravimetric studies of Fe(III) complexes were carried out from room temperature to 800°C. The stages of decomposition, temperature range, decomposition products as well as mass percentage loss of all Fe(III) complexes found. The TG-DTG graphs of [Fe $L^1{}_2$]Cl_3, [Fe $L^2{}_2(H_2O)Cl$] and [Fe$L^3{}_2(H_2O)Cl$] are given in Figure 1,2,3 respectively. The results shows good agreement with the theoretical formula as suggested from analytical data [24, 27]. The data revealed following findings; [Fe $L^1{}_2$]Cl_3 shows single stage decomposition. The complex is found to be stable up to 210°C. Beyond 210°C, it decomposes in single stage. The decomposition starts at 210°C and ends at 400 °C. The mass loss has a peak temperature of 270° C. The mass percentage of Fe is found to be 6.90% which further confirms the stoichiometry. The final residue is obtained at a temperature of 510°C that corresponds to iron oxide.

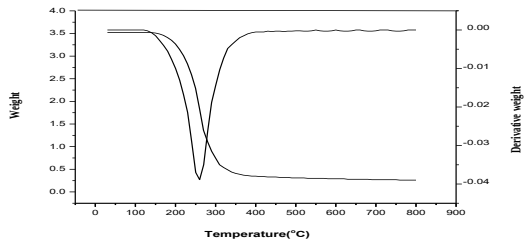

***Figure 1**. TG/DTG of [Fe $L^1{}_2$]Cl_3.*

In the case of [Fe $L^2{}_2(H_2O)Cl$], the complex is found to be stable up to 180°C. The first stage decomposition starts at 190°C and ends at 215°C. The mass loss is 2.7% with a corresponding peak temperature of 210 °C may be attributed to liberation of coordinated water molecule.

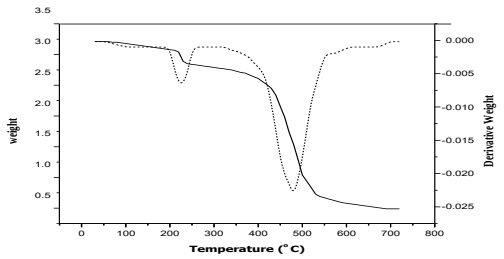

***Figure 2**. TG/DTG of [Fe $L^2{}_2(H_2O)Cl$].*

The second stage starts around 400°C and ends at 680°C. This mass loss is mainly due to loss of chloride ion and two molecules of L^2 which has a peak temperature of 550°C. The mass percentage of Fe is found to be 8.90% which further confirms the stoichiometry. The decomposition is continuous and relatively slow. The final residue of Fe_2O_3 is obtained at a temperature of 680 °C.

The TG-DTG graph of [Fe $L^3{}_2(H_2O)Cl$] also shows two stage decomposition. This complex is stable up to 150°C. The decomposition shows mainly two stages.

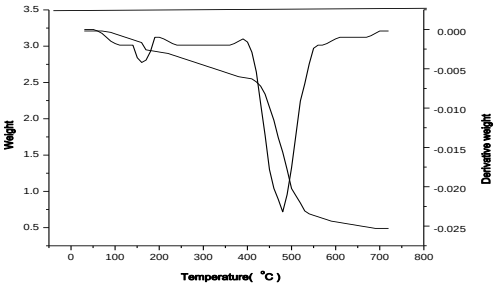

***Figure 3**. TG/DTG of [Fe $L^3{}_2(H_2O)Cl$].*

The first stage starts at 160°C and ends at 220°C. This may be due to loss of coordinated water molecule that comes to 2.17%. The second stage starts at 270°C and ends at 550°C. The second stage decomposition is continuous and relatively slow. The final stage involves decomposition of chloride ion and two molecules of L^3 moiety which has a peak temperature of 390°C. The residue corresponds to Fe_2O_3 which is obtained at 700°C. The mass percentage of Fe is found

to be 6.71% which further confirms the stoichiometry.

3.2 IR Spectra of Iron Oxide

IR analysis was employed to confirm the transformation of Fe(III) chelates to iron oxide during the thermal treatments. In order to find out the type of iron oxide formed on thermal decomposition the infrared spectra of iron oxide in the range 400-750 cm^{-1} were analyzed. The absorption bands in range 400-750 cm^{-1} represent Fe-O vibration mode [30]. The iron oxide formed can exist mainly in different polymorphs, hametite (α-Fe_2O_3), magnetite (Υ- Fe_2O_3), other polymorph designated as β- Fe_2O_3 which is very rarely found and Fe_3O_4. For Fe_3O_4 there is only one peak seen around 574 cm^{-1}. For Υ-Fe_2O_3 three peaks can be seen in range 500 – 700cm^{-1}. For α-Fe_2O_3 two peaks are seen around in range 500 – 700cm^{-1} [31]. The represented FTIR spectra confirms the transformation of Fe(III) complexes to α-Fe_2O_3 on thermal decomposition.

IR spectra of residue obtained from $[FeL^1_2]Cl_3$, $[FeL^2_2(H_2O)Cl]$ and $[FeL^3_2(H_2O)Cl]$ is given in Figure 4,5,6 respectively.

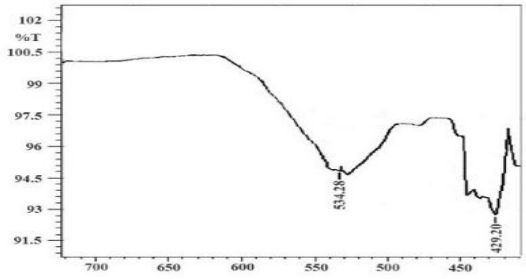

Figure 4. *IR spectrum of iron oxide obtained from* $[Fe\ L^1_2]Cl_3$.

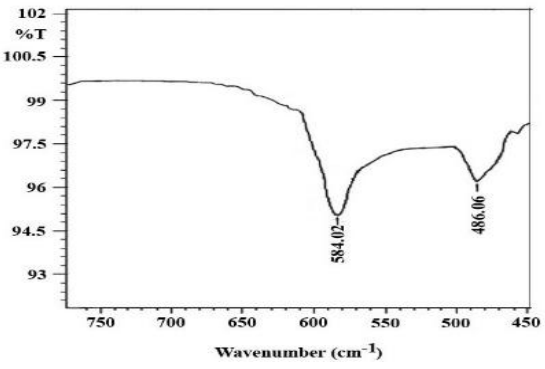

Figure 5. *IR spectrum of iron oxide obtained from* $[FeL^2_2(H_2O)Cl]$.

The IR spectrum of iron oxide obtained from $[FeL^1_2]Cl_3$ shows two peaks at 534 and 429 cm^{-1}. The residue obtained from $[FeL^2_2(H_2O)Cl]$ shows two peaks at 584 and 486 cm-1 and that from $[FeL^3_2(H_2O)Cl]$ also shows two peaks at 580 and 545 cm^{-1} attributed to Fe-O stretching and O-Fe-O bending vibration modes of iron oxide that corresponds to α-Fe_2O_3 [28, 29].

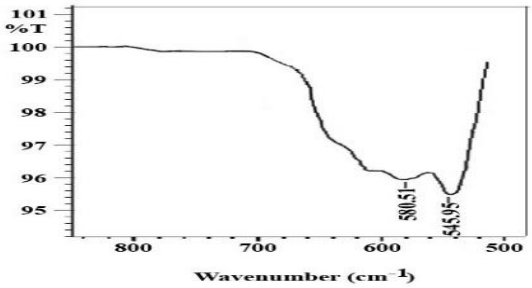

Figure 6. *IR spectrum of iron oxide obtained from* $[FeL^3_2(H_2O)Cl]$.

From IR spectral evidences it is confirmed that iron oxide obtained from different chelates are of type α-Fe_2O_3 [32]. The presence of low intensity bands in addition to the desired peak can be due to the remnants of undecomposed parent compounds.

3.3 Powder X-Ray Diffraction Analysis of the Iron Oxide Residue

The X-ray powder method is a finger print method used to characterize and check the purity of crystalline materials. Here we have done XRD analysis of newly synthesized iron nanoparticles to evaluate the size of nanoparticles and its crystalline nature. Data was compared with JCDPS file.

The powder X-ray diffraction (XRD) pattern recorded for the prepared iron oxide from thermal decomposition of complex $[FeL^1_2]Cl_3$ is shown in Figure.7. The XRD diffraction pattern peak of iron oxide nanoparticles obtained was

compared with the standard [JCDPS file No.33-0664] and it shows that metal oxide are in pure α-Fe_2O_3 form. The diffraction peak corresponding to (012) (104) (110) (113) (024) (116) (214) (300) (1010) are quite identical to characteristic peaks of α-Fe_2O_3 crystals. The XRD diffraction pattern peaks of Fe_2O_3 become narrower with prolonging reaction time and narrow peaks suggested that α-Fe_2O_3 samples are highly crystalline and is testified that iron oxide nano crystalline could be synthesized through this method [34, 35].

Average particle size have been calculated from high intensity peak using the Debye -Scherrer equation.

$$d = \frac{0.89\lambda}{\beta \cos\theta}$$

Where λ is wavelength of X-ray radiation, β is the full width at half maximum intensity in radians and θ is angle of diffraction [36]. From the XRD data, particle size calculated is 69 nm. The (110) peak is used for calculation.

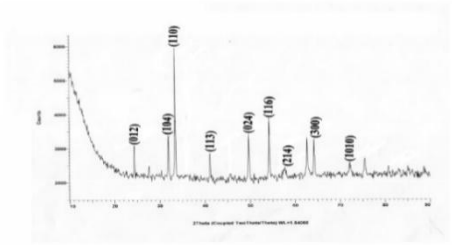

Figure 7*. XRD pattern of iron oxide obtained from [FeL^1_2]Cl_3.*

The powder X-ray diffraction (XRD) pattern recorded for the prepared iron oxide from thermal decomposition of complex [$FeL^2_2(H_2O)Cl$] is shown in Figure 8. The XRD diffraction pattern peak of iron oxide nanoparticles obtained was compared and it shows that metal oxide are in pure α-Fe_2O_3 form. From the XRD data, particle size calculated is 78 nm using this equation. The (104) peak is used for calculation.

The powder X-ray diffraction (XRD) pattern recorded for the prepared iron oxide from thermal decomposition of complex [$FeL^3_2(H_2O)Cl$] is shown in Figure 9.

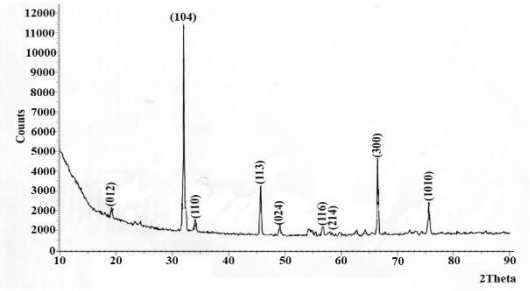

Figure 8*. XRD pattern of iron oxide obtained from [$FeL^2_2(H_2O)Cl$].*

From the XRD data, particle size calculated is 121 nm. The (110) peak is used for calculation.

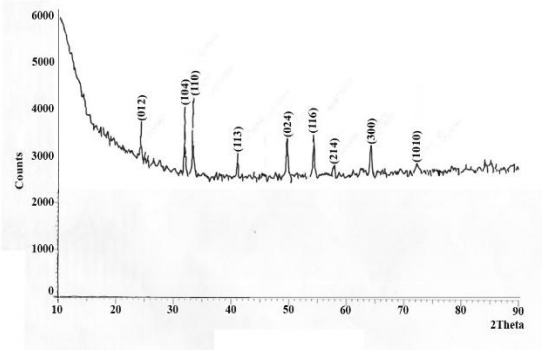

Figure 9*. XRD pattern of iron oxide obtained from [$FeL^3_2(H_2O)Cl$].*

3.4 VSM Measurement

The magnetic characterization of nanoparticles was done using vibrating sample magnetometer at room temperature with a magnetic field in the range -10000 to 10000 Oe. VSM of iron oxide nanoparticles carried out at room temperature obtained by the decomposition of [$FeL^2_2(H_2O)Cl$] shows hysteresis behavior (M-H loop), relation between the induced magnetic flux density and magnetization force. The curve shows saturation magnetization at 10.360 x 10^{-3} emu/g with a coercive force of 2811.8 G and retentivity 3.683 x 10^{-3} emu representing ferromagnetic behavior in nano crystalline form [37]. The VSM of iron oxide nanoparticles obtained from [Fe $L^2_2(H_2O)Cl$] is shown in Fig. 10.

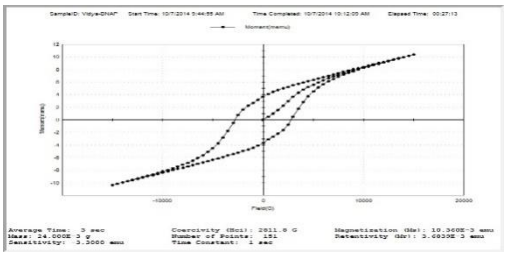

Figure 10*. VSM graph of iron oxide obtained from [FeL$^2_2$(H$_2$O)Cl].*

3.5 Morphological Characterization of Iron Oxide Nanoparticles

Morphology of the prepared iron oxide was characterized by SEM and TEM analysis [38, 39, 40, 41].

3.5.1 FEG-SEM Analysis of Iron Oxide

SEM micrograph of iron oxide residue obtained by heating [FeL$^2_2$(H$_2$O)Cl] and [Fe L$^3_2$(H$_2$O)Cl] were taken. Iron oxide nanoparticles obtained from [Fe L$^2_2$(H$_2$O)Cl] at 680^{o}C for about 20 minutes, shows rod shaped, flakes like and sphere like particles. Both aggregated particles and voids are seen. The SEM images of iron oxide nanoparticles from [Fe L$^2_2$ (H$_2$O)Cl] are given in Figure 11.

The SEM micrograph of the decomposition product of the complex [Fe L$^3_2$(H$_2$O)Cl] heated at 700^{o}C shows particles in the range 19, 30, 65, 64.3, 69, 80.4, 84.7 nm. The aggregation of particles are clearly seen. Voids are also seen in between. The SEM image shows spherical particles in above dimensions. SEM images of [Fe L$^3_2$(H$_2$O)Cl] are given in Figure 12.

3.5.2 TEM Analysis

TEM micrograph of the iron oxide obtained by thermal decomposition of [Fe L$^1_2$]Cl$_3$ heated at 510^{o}C shows shows nano particles having size in the range 21 – 50 nm. The figure shows spherical particles with narrow size distribution. The TEM image of iron oxide obtained from [FeL$^1_2$ (H$_2$O)Cl] is shown in Figure 13.

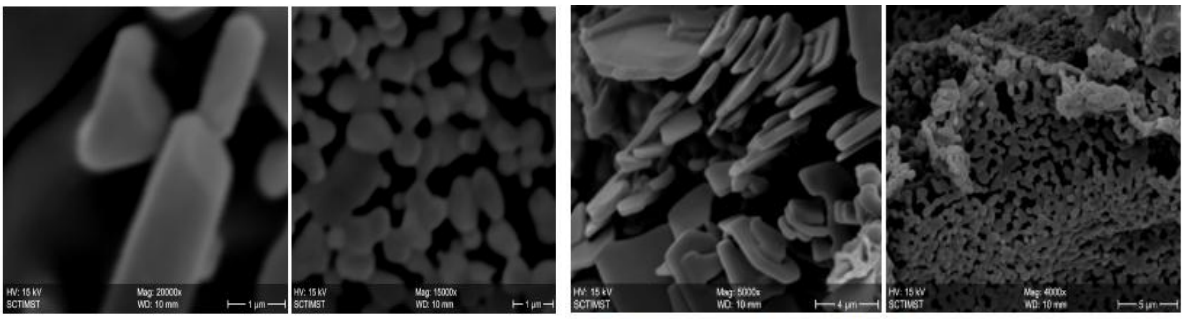

Figure 11*. SEM images of iron oxide obtained from[Fe L$^2_2$(H$_2$O)Cl] heated at 680^{o}C.*

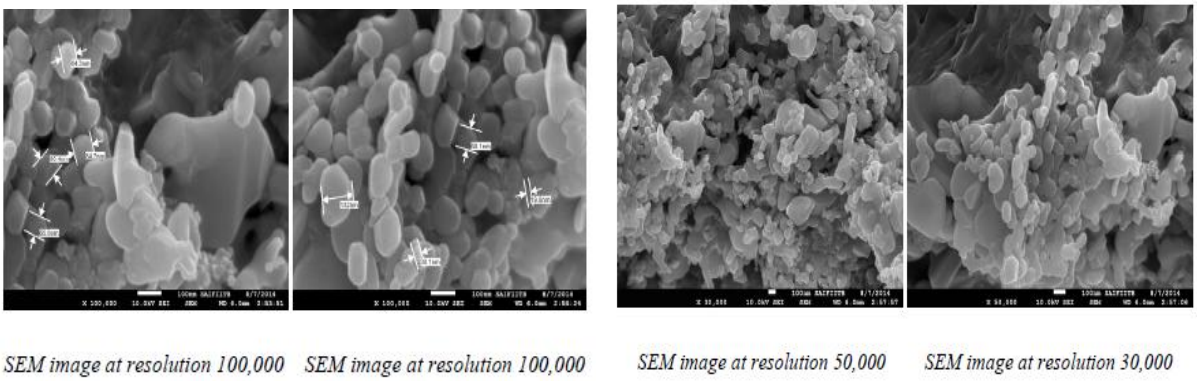

Figure 12*. SEM images of iron oxide obtained from[Fe L$^3_2$(H$_2$O)Cl] heated at 700^{o}C.*

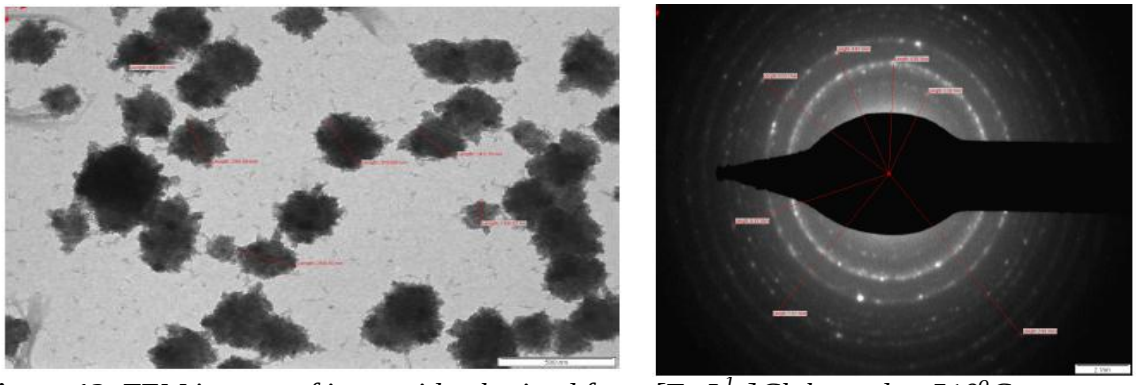

Figure 13. *TEM images of iron oxide obtained from* $[Fe\ L^1{}_2]Cl_3$ *heated at* 510^oC

4. CONCLUSION

The study demonstrates that the nano sized α-Fe_2O_3 particles with good homogeneity in size can be prepared by thermal decomposition of iron complexes. The physical property analysis of iron oxide nanoparticles studied by XRD, VSM and FTIR analysis and surface morphological analysis by SEM and TEM. XRD analysis show that iron oxide was formed as α-Fe_2O_3 instead of commonly formed magnetite nanoparticle, Fe_3O_4 or a mixture of magnetite and maghemite. VSM studies shows that iron oxides exhibit ferromagnetic behavior. It is believed that this approach may be extended to synthesize other metal oxide nano structures. The particles obtained by thermal decomposition needs some treatment for purification and also for obtaining close uniformity.

ACKNOWLEDGEMENTS

The authors are thankful to SAIF, IIT Mumbai and Chennai, SCT Poojappura for the availed facilities and Department of Chemistry, University College, Trivandrum for instrumental facilities under DST FIST.

I author is thankful to UGC for the FDP support.

CONFLICT OF INTEREST

The authors declare that they have no conflict of interest.

REFERENCES

1. Laurent, S., Forge, D., Port, M., Roch, A., Robic, C., Elst, L. V., Muller, R. N., (2008). "Magnetic iron oxide nanoparticles: synthesis, stabilization, vectorization, physicochemical characterizations, and biological applications", *Chem. Rev.,* 108(6): 2064-110.
2. Gupta, A. K., Gupta, M., (2005). "Synthesis and surface engineering of iron oxide nanoparticles for biomedical applications", *Biomat.,* 26(18): 3995-4021.
3. Park, J., Joo, J., Kwon, S. G., Jang, Y., Hyeon, T., (2007). "Synthesis of monodisperse spherical nanocrystals", *Angew. Chem. Int. Ed*. *Engl*., 46(25): 4630-60.
4. Patel, D., Moon, J. Y., Chang, Y., Kim, T. J., Lee, G. H., (2008). "Poly (d,l-lactide-co-glycolide) coated superparamagnetic iron oxide nanoparticles: Synthesis, characterization and in vivo study as MRI contrast agent". *Colloid Surf. A,* 9: 313-314.
5. Lu, A. H., Salabas, E. L., Schuth, F., (2007). "Magnetic nanoparticles: synthesis, protection, functionalization, and application", *Angew. Chem. Int. Ed.* Engl., 46(8): 1222-44.
6. Jun, Y. W., Lee, J. H., Cheon, J. W., (2008). "Chemical design of nanoparticle probes for high-performance magnetic resonance imaging", *Angew. Chem. Int. Ed*. Engl., 47(28): 5122-35.
7. Corot, C., Robert, P., Idee, J. M., Port, M., (2006). "Recent advances in iron oxide nanocrystal technology for medical imaging", *Adv. Drug. Deliv. Rev*., 58: 1471-1504.
8. Wang, Y. X. J., Hussain, S. M., Krestin, G. P., (2001). "Superparamagnetic iron oxide contrast agents: physicochemical characteristics and applications in MR imaging", *Eur. Radiol.,* 11(11): 2319-31.
9. Gupta, A. K., Naregalkar, R. R., Vaidya, V. D., Gupta, M., (2007). "Recent advances on surface engineering of magnetic iron oxide nanoparticles and their applications", *Nanomedicine,* 2(1): 23-39.

10. Patel, D., Moon, J. Y., Chang, Y., Kim, T. J., Lee, G. H., (2008). "Poly (d,l-lactide-co-glycolide) coated superparamagnetic iron oxide nanoparticles: Synthesis, characterization and in vivo study as MRI contrast agent", *Colloid Surf. A*, 91: 313-314.
11. Zhao, M., Josephson, L., Tang, Y., Weissleder, R., (2003). "Magnetic sensors for protease assay". *Angew. Chem. Int. Ed*., 42(12): 1375 -8.
12. Mornet, S., Vassear, S., Grasset, F., Veverka, P., Goglio, G., Demourgues, A., (2006). "Magnetic nanoparticle design for medical applications", *Prog. Solid state Chem.,* 34(2): 237-247.
13. Stevens, P. D., Fan, J., Gardimalla, H. M. R., Yen, M., Gao, Y., (2005). "Superparamagnetic nanoparticle-supported catalysis of Suzuki cross-coupling reactions". *Org. Lett.,* 7(11): 2085- 8.
14. Jun, Y., Choi, S. J., Cheon, J., (2007). "Heterostructured magnetic nanoparticles: their versatility and high performance capabilities", *Chem. Commun. (Camb),* 12: 1203-14.
15. Cornell, R. M., Schwertmann, U., (2003). "*The iron oxides: Strucures, Properties, Reactions occurences and uses*". Wiley- VCH, Weinheim.
16. Nami, N., Lale Mohammadi, S., (2017). "One-Pot Facile Synthesis of New 1, 2, 4-Triazolidine Derivatives Using $NaBH_4$ and Fe_3O_4 Magnetic Nanoparticles", *Int. J. Nanosci. Nanotechnol.*, 13(4): 347-357.
17. Iqbal, T., Tufail, S., Ghazal, S., (2017). "Synthesis of Silver, Chromium, Manganese, Tin and Iron Nano Particles by Different Techniques", *Int. J. Nanosci. Nanotechnol.*, 13(1): 19-52.
18. Daou, T. J., Pourroy, G., Begin-Colin, S., Greneche, J. M., Ulhaq-Bouillet, *C.*, (2010). "Hydrothermal Synthesis of Monodisperse Magnetite Nanoparticles", *Chem. Mater.*, 18: 4399-4404.
19. Hyeon, T., Lee, S. S., Park, J., Chung, Y., Bin Na, H., (2001). "Synthesis of highly crystalline and monodisperse maghemite nanocrystallites without a size ultra large synthesis of monodisperse nanocrystals", *J. Am. Chem. Soc*., 123(51): 12798-12801.
20. Hyeon, T., (2003). "Chemical synthesis of magnetic nanoparticles" *Chem . Commun.;* 50: 927-934.
21. Park, J., An, K., Hwang, N. M., Park, J. G., Noh, H. J., Kim, J. Y., Park, J. H., Hwang, N. M., Hyeon, T., (2004). "Ultra-Large Scale Syntheses of Monodisperse nano crystals", *Nat. Mater*., 3(12): 891-895.
22. Benyettou, F., Hardouin, J., Marc, L., Jouni, H., Motte, L., (2012). "PEGylated versus non-PEGylated Fe_2O_3@Aldendronate Nanoparticles". *J. Bioanal. Biomed.*, 4: 39-45.
23. Sadasivan, V., Alaudeen, M., (2007). "Synthesis and crystal structure of Zinc(II) complex of 5-(2,3-dimethyl-1-phenyl-3-pyrazolin-5-one-4-yihydrazono)hexahydropyramidin-2-thioxo-4,5,6-trione". *Indian J. Chem.,* 46(A): 1959-1962.
24. Vidya, V.G., Meena, S. S., Pramod Bhatt., Sadasivan, V., Mini, S., (2013). "Spectroscopic studies on Fe(II) and Fe(III) complexes of 5-aryl azo substituted lH-pyrimidine-2,4-dione", *AIP Conf. Proc.,* 1536: 1009-1011.
25. Mini, S., Meena, S. S., Pramod Bhatt., Sadasivan, V.. Vidya, V. G., (2013). "Synthesis and characterization of Fe (III) complex of an azo dye derived from (2-amino-5-chlorophenyl) phenyl methanone", *AIP Conf. Proc*., 1536: 1011-1014.
26. Vidya, V. G., Sadasivan, V., (2018). "Synthesis and Charaterisation of Metal chelates of (5-(2,3-dimethyl-1-phenyl-3-pyrazolin-5-one-4-ylazo)-^{1}H-pyrimidine-2,4-dione)". *Journal of Ultra Chemistry*, 14(2): 57-68.
27. Vidya, V.G., Meena, S. S., Pramod Bhatt., Sadasivan, V., (2014). "Synthesis and spectral study of new azo dye and its iron complexes derived from 2- naphthol and 2-amino-3-hydroxypyridine". *AIP Conf. Proc.,* 1620: 622- 626.
28. Mini, S., Meena, S. S., Pramod Bhatt., Sadasivan, V., (2014). "Spectroscopic studies on two mono nuclear iron (III) complexes derived from a Schiff base and an azodye", *AIP Conf. Proc*., 1620: 322-326.
29. Mini, S., Sadasivan, V., Meena, S. S., Pramod Bhatt., (2015). "Synthesis and studies of metal complexes of a Schiff base derived from (2-amino-5-chlorophenyl)phenyl methanone', *Spectrochim. Acta A*, 151: 598-604.
30. Vidya, V. G., Sadasivan, V., (2018). "Synthesis, spectral and biological studies of complexes with bidentate azodye ligand derived from resorcinol and 1-amino-2-naphthol-4-sulphonic acid". *Orient. J. Chem.,* 34(1): 45-54.
31. Battisha, J. K., Afify, H. H., Ibrahim, M., (2006). "Synthesis of Fe_2O_3. Concentrations and Sintering Temperature on FTIR and *Magnetic*. Susceptibility Measured From 4 to 300 K of Monolith Silica Gel. Prepared by Sol-Gel Technique", *J. Magn. Magn. Mat.,* 306: 211-215.
32. Zhao, B., Wang, Y., Guo, H., He, Y., Jiao, Z., Wu, M., (2007). "Iron oxide(III) nanoparticles fabricated by electron beam irradiation method", *Mat. Sci.,* 25: 1143-1148.
33. Xiang wei, M., Tung, W., Shiwei, S., Rongbo, Z., Jun, R., Fanggiong, T., (2010). "Synthesis and applications of carbon iron oxide microspheres. Black pigments in electrophoretic displays", *Nanoscale Res. Lett.,* 5(10): 1664-1668.
34. Xiao-Quan, Chen, Shi- Bin, Wu., Ren-Bo, Cao., Jin-Song, Tao., (2014). "Preperation and characterization of nanosized hematite colloids using green vitriol as ferrum source", *J. nano mtrls.,* 749-562.

35. Ning, Du., Yan Fang, X., Hui, Z., Chuanxin, Z., Deven, Y., (2010). "Selective synthesis of FeO nanowires via single precursor. A general method for metal oxide", *Nano Scale Res.* Lett., 5: 1295-1300.
36. Lemine, O. M., (2009). "Microstructural characterisation of α-FeO nanoparticles using, XRD line profiles analysis, FE-SEM and FT-IR", *Super Lattice Microst.,* 45: 576-582.
37. Avnish, K. A., Mohan, S., Ritu, K., Vivek, S., Pakaj, K., (2014). "Synthesis, characterization and magnetic studies of nanoparticles", *J. Nanotech.,* 47: 4909-4916.
38. Vidya, V. G., Revathy, L., (2018). "Synthesis and Characterization Of Calcium Ferrite Nanoparticles By Solution Combustion Method", *Bulletin of Pure and Applied Science- Chemistry,* 37C(1): 131-136.
39. Suriyaprabha, R. S. H., Khan, B. P., Fulekar, M. H., (2017). "Spherical Surfaced Magnetic **N**Ps as Nano Adsorbent Material ,for Treatment of Industrial Dye Effluents", *Int. J. Nanosci. Nanotechnol,* 13(2): 169-175.
40. Honary, S., Ebrahimi, P., Asgari-rad, H., Mohamadpour, F., (2014). "Optimization of IONPS Preparation for Biomedical Applications", *Int. J. Nanosci. Nanotechnol.,* 10(4): 257-261.
41. Mohammadi, S. Z., Khorasani-Motlagh, M., Sh. Jahani, ousefi, M., (2012). "Synthesis and Characterization of α-Fe_2O_3 Nanoparticles by Microwave Method", *Int. J. Nanosci. Nanotechnol.,* 10(4): 257-261.